Available online at www.sciencedirect.com
SCIENCE DIRECT
International Journal of Heat and Mass Transfer 49 (2006) 2703–2711
International Journal of HEAT and MASS TRANSFER
www.elsevier.com/locate/ijhmt

System performance of a combined heat and mass recovery adsorption cooling cycle: A parametric study

K.C. Leong *, Y. Liu

School of Mechanical and Aerospace Engineering, Nanyang Technological University, 50 Nanyang Avenue, Singapore 639798, Republic of Singapore

Received 22 April 2005; received in revised form 9 January 2006
Available online 9 March 2006

Abstract

Based on the previous work of the authors [K.C. Leong, Y. Liu, Numerical study of a combined heat and mass recovery adsorption cooling cycle, Int. J. Heat Mass Transfer 47 (2004) 4761–4770], a numerical study of the effects of system design and operation parameters on the performance of a combined heat and mass recovery adsorption cycle is presented in this paper. The effects of bed dimensions, bed thermal conductivity, heat exchange fluid velocity, driven temperature and the degree of the heat recovery on the system performance are investigated. It is found that an increase in the driven temperature results in the increase of both the coefficient of performance (COP) and specific cooling power (SCP) of the adsorption cycle. On the other hand, the system performance can be severely deteriorated for velocities of the heat exchange fluid smaller than a critical value. An increase in the bed thickness will result in an increase in COP and a decrease in the SCP. The results of our simulations will provide useful guidelines for the design of this type of advanced adsorption cooling cycle.

Keywords: Adsorption; Adsorbent; Cooling; Heat and mass recovery; Numerical study

1. Introduction

The environmental-friendly adsorption cooling system is an attractive alternative to the traditional CFC-based vapor-compression cooling system as it employs safe and non-polluting refrigerants. Another advantage of adsorption cooling systems is that they can be driven by low-grade energy such as waste heat or solar energy. As a result, adsorption cooling systems have attracted much research attention in recent years.

However, the widespread application of adsorption systems is limited by its rather low coefficient of performance (COP), low specific cooling power (SCP) and long cycle time. In order to improve the performance of the adsorption cooling system, some advanced cycles have been proposed and investigated, such as the continuous cycle [1,2], the forced convection cycle [3] and the thermal wave cycle [4]. The forced convection and thermal wave cycles are both capable of achieving high COP values. However, these systems are inherently more complicated and are not suitable for actual engineering applications. The continuous cycle that incorporates heat and mass recovery cycles is verified to be a simple and effective method to improve the thermal performance [5]. The heat recovery cycle serves to recover thermal energy from the temperature difference between the two adsorbent beds while mass recovery can increase the cycled refrigerant mass, which leads to improved performance. In order to achieve better performance, heat regeneration and mass recovery should be simultaneously employed.

Thermodynamic investigations of the two-bed heat and mass recovery adsorption cycle have been carried out in recent years by several researchers [5–7]. Although these researchers obtained some good results, their models gave only the COP values without any information of the transient heat and mass transfer processes. Poyelle et al. [8] proposed a simple one-dimensional numerical model for a heat

* Corresponding author. Tel.: +65 6790 4725; fax: +65 6792 2619.
E-mail address: mkcleong@ntu.edu.sg (K.C. Leong).

0017-9310/$ - see front matter © 2006 Elsevier Ltd. All rights reserved.
doi:10.1016/j.ijheatmasstransfer.2006.01.012

Nomenclature

C_p	specific heat (J kg^{-1} K^{-1})
COP	coefficient of performance
d	particle diameter (m)
D_e	equivalent diffusivity in the adsorbent particles (m^2 s^{-1})
D_h	degree of heat recovery (%)
K_{ap}	apparent permeability (m^2)
L	length of adsorbent bed (m)
m	mass (kg)
P	pressure (Pa)
$\bar{q}$	adsorbed amount (kg kg^{-1})
r	radial coordinate (m)
r^*	dimensional radial coordinate (m)
R	universal gas constant (J kmol^{-1} K^{-1}); adsorber radius (m)
SCP	specific cooling power (W kg^{-1})
t	time (s)
t_c	cycle time (s)
t_h	heat recovery time (s)
T	temperature (K)
T_a	initial adsorption temperature of adsorbent bed (K)
T_g	generation temperature of adsorbent bed (K)
u	vapor velocity in axial direction (m s^{-1})
u_f	fluid velocity (m s^{-1})
$\bar{u}_f$	average fluid velocity (m s^{-1})
u_f^*	dimensional fluid velocity
$\boldsymbol{u}$	vapor velocity vector (m s^{-1})
u^*	dimensional vapor velocity in axial direction
v	vapor velocity in radial direction (m s^{-1})
v^*	dimensional vapor velocity in radial direction
z	axial direction (m)
z^*	dimensional axial coordinate

Greek symbols

ΔH	heat of adsorption (J kg^{-1})
ε	total porosity
ε_a	macro-porosity
ε_i	micro-porosity
λ	thermal conductivity (W m^{-1} K^{-1})
μ	dynamic viscosity (N s m^{-2})
θ	dimensional temperature
τ	dimensional time
ρ	density (kg m^{-3})
ω	dimensional pressure
Ω	dimensional adsorbed amount

Subscripts

a	adsorbed phase
c	condensing; cooling
e	evaporating
eq	equivalent
f	external heating exchange fluid
g	water vapor
h	heating
in	inlet fluid
m	metal tube
s	adsorbent
R	reference

and mass recovery adsorption-based air conditioning cycle. Although their model fitted the experimental data very well, there was a need to specify some empirical parameters a priori. Recently, Leong and Liu [9] presented a two-dimensional heat and mass transfer model of a combined heat and mass recovery adsorption cycle. They obtained COP values for a compact zeolite bed-based cycle which are 47% larger than the single bed cycle.

In this paper, the effect of design and operating parameters on the thermal performance of a zeolite/water combined heat and mass recovery cycle is presented based on a two-dimensional heat and mass transfer model proposed by the authors [9]. The simulation results will provide useful information for the design and operation of this advanced cycle.

2. Numerical model

The combined heat and mass recovery adsorption cycle shown in Fig. 1 has been described in detail in a previous paper by the authors [9]. The numerical model focuses on the heat and mass transfer phenomena in the two adsorbers. A schematic of the adsorbers is shown in Fig. 2. The adsorber is a hollow cylinder which encloses a metal tube for the purpose of heat exchange between the solid adsorbent and the heating or cooling fluid within the tube.

The following assumptions are made:

(1) The adsorbed phase is considered as a liquid and the adsorbate gas is assumed to be an ideal gas.
(2) The adsorbent bed is composed of uniform-size particles and has isotropic properties.
(3) The properties of the fluid, the metal tube and adsorbate vapor are constant.
(4) There are no heat losses in the adsorption cycle.
(5) The thermal resistance between the metal tube and the adsorbent bed is neglected. This is consistent with the findings of Zhu and Wang [10] who showed that the contact thermal resistance is only equivalent to a 0.4 mm-thick adsorbent used in our model.
(6) The velocity distribution is assumed to be parabolic in the radial direction and remains constant in the

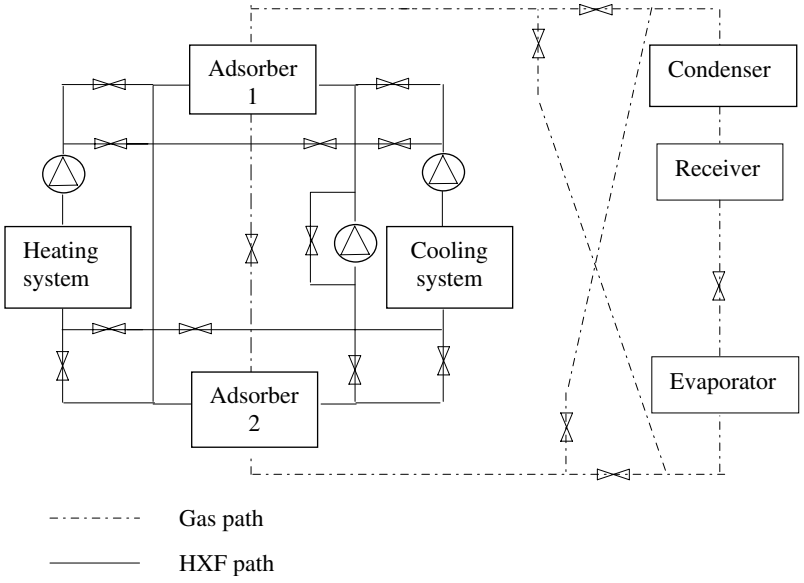

Fig. 1. Schematic diagram of two-bed adsorption refrigeration system with heat and mass recovery.

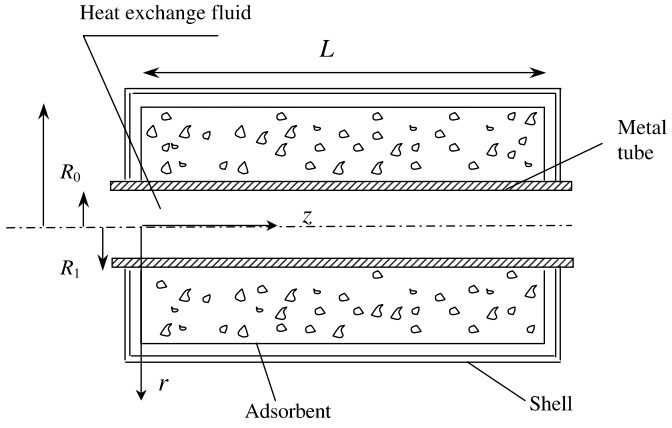

Fig. 2. Schematic diagram of the adsorber.

axial direction. In addition, flow resistance arising from the water flowing in the pipeline is neglected.

(7) The pressure in condenser or evaporator during the entire adsorption cycle is kept as a constant value.

The energy equations for different components of the two adsorbers can be developed as follows:

The energy balance on the thermal-fluid system yields

$$\frac{\partial(\rho_f C_{pf} T_f)}{\partial t} + \frac{\partial(\rho_f C_{pf} u_f T_f)}{\partial z} = \frac{\partial}{\partial z}\left(\lambda_f \frac{\partial T_f}{\partial z}\right) + \frac{1}{r}\frac{\partial}{\partial r}\left(r\lambda_f \frac{\partial T_f}{\partial r}\right) \quad (1)$$

The energy balance for the metal tube is given by

$$\frac{\partial(\rho_m C_{pm} T_m)}{\partial t} = \frac{\partial}{\partial z}\left(\lambda_m \frac{\partial T_m}{\partial z}\right) + \frac{1}{r}\frac{\partial}{\partial r}\left(r\lambda_m \frac{\partial T_m}{\partial r}\right) \quad (2)$$

The energy balance for the adsorbent can be written as

$$(\rho_s C_{p_s} + \rho_s q C_{pa} + \varepsilon\rho_g C_{pg})\frac{\partial T_s}{\partial t} + \frac{\partial(\rho_g C_{pg} u T_s)}{\partial z} + \frac{1}{r}\frac{\partial}{\partial r}(r\rho_g C_{pg} v T_s) = \frac{\partial}{\partial z}\left(\lambda_{eq}\frac{\partial T_s}{\partial z}\right) + \frac{1}{r}\frac{\partial}{\partial r}\left(r\lambda_{eq}\frac{\partial T_s}{\partial r}\right) + \rho_s \Delta H \frac{\partial \bar{q}}{\partial t} \quad (3)$$

where subscripts f, m and s denote the heat exchange fluid, metal tube and adsorbent, respectively. The linear driven force (LDF) model is used for describing the adsorption rate as

$$\frac{\partial \bar{q}}{\partial t} = \frac{15 D_e}{r_p^2}(q_{eq} - \bar{q}) \quad (4)$$

where q_{eq} is the adsorbed phase concentration in equilibrium with bulk fluid for zeolite NaX/water pair, which is defined as the sum of three Langmuir terms stated by Ben Amar et al. [11].

The overall mass conservation in the adsorber is

$$\frac{\partial \varepsilon \rho_g}{\partial t} + \nabla \cdot (\rho_g \boldsymbol{u}) + \rho_s \frac{\partial \bar{q}}{\partial t} = 0 \quad (5)$$

Substituting the modified Darcy's equation in the literature [9] into Eq. (5) for simplicity of calculation, we obtain

$$\frac{\partial\left(\frac{\varepsilon M}{RT}P\right)}{\partial t} = \frac{\partial}{\partial z}\left(\frac{\rho_g K_{ap}}{\mu}\frac{\partial P}{\partial z}\right) + \frac{1}{r}\frac{\partial}{\partial r}\left(\frac{r\rho_g K_{ap}}{\mu}\frac{\partial P}{\partial r}\right) - \rho_s \frac{\partial \bar{q}}{\partial t} \quad (6)$$

The initial and boundary conditions are listed below to complete the numerical formulation of the problem.

Initial conditions:

For $t = 0$ $T_f(z,r) = T_{cin}$; $T_m(z,r) = T_s(z,r) = T_{a2}$
$P = P_e$ (Adsorber 1) (7)

For $t = 0$ $T_f(z,r) = T_m(z,r) = T_s(z,r) = T_{g2}$
$P = P_c$ (Adsorber 2) (8)

Boundary conditions:

$$\left.\frac{\partial T_f}{\partial z}\right|_{z=0} = \left.\frac{\partial T_f}{\partial z}\right|_{z=L} = 0 \quad \text{during mass recovery phase} \tag{9}$$

$$T_{f1}|_{z=0} = T_{f2}|_{z=L}; \quad T_{f2}|_{z=0} = T_{f1}|_{z=L}$$
during heat recovery phase (10)

$$T_f|_{z=0} = T_{hin}$$
when connected to external heating system (11)

$$T_f|_{z=0} = T_{cin}$$
when connected to external cooling system (12)

$$\left.\frac{\partial T_m}{\partial z}\right|_{z=0} = \left.\frac{\partial T_m}{\partial z}\right|_{z=L} = 0 \tag{13}$$

$$\left.\frac{\partial T_s}{\partial z}\right|_{z=0} = \left.\frac{\partial T_s}{\partial z}\right|_{z=L} = \left.\frac{\partial T_s}{\partial r}\right|_{r=R} = 0 \tag{14}$$

$$P_1|_{z=0} = P_1|_{z=L} = P_1|_{r=R=P_a}$$
during mass recovery phase for Adsorber 1 (15)

$$P_2|_{z=0} = P_2|_{z=L} = P_2|_{r=R=P_a}$$
during mass recovery phase for Adsorber 2 (16)

$$\left.\frac{\partial P}{\partial z}\right|_{z=0} = \left.\frac{\partial P}{\partial z}\right|_{z=L} = \left.\frac{\partial P}{\partial r}\right|_{r=R} = 0 \tag{17}$$

$$P|_{z=0} = P|_{z=L} = P|_{r=R} = P_e$$
when connected to evaporator (18)

$$P|_{z=0} = P|_{z=L} = P|_{r=R} = P_c$$
when connected to condenser (19)

where the symbols with subscripts 1 and 2 represent the properties of Adsorbers 1 and 2, respectively. Otherwise, these boundary conditions are suitable for the two adsorbers. P_a is the pressure in the space between the adsorbent and the shell during the mass recovery phase, and it is assumed to be equal for the two adsorbers during the mass recovery phase. P_a can be calculated from the mass conservation equation by using an iteration technique [9].

To simplify the solution of the governing equations, the heat and mass conservation equations in this numerical model can be re-written in dimensionless forms. The resulting dimensionless equations are

$$\frac{\partial \theta_f}{\partial \tau} + u_f^* \frac{\partial \theta_f}{\partial z^*} = \frac{\partial}{\partial z^*}\left(\frac{1}{Pe_f}\frac{\partial \theta_f}{\partial z^*}\right) + \frac{1}{Ar^2}\cdot\frac{1}{r^*}\frac{\partial}{\partial r^*}\left(\frac{r^*}{Pe_f}\frac{\partial \theta_f}{\partial r^*}\right) \tag{20}$$

$$\frac{\partial \theta_m}{\partial \tau} = \frac{\partial}{\partial z^*}\left(\frac{1}{Pe_m}\frac{\partial \theta_m}{\partial z^*}\right) + \frac{1}{Ar^2}\cdot\frac{1}{r^*}\frac{\partial}{\partial r^*}\left(\frac{r^*}{Pe_m}\frac{\partial \theta_m}{\partial r^*}\right) \tag{21}$$

$$(1 + r_a\Omega + r_g)\frac{\partial \theta_s}{\partial \tau} + r_g\left(u^*\frac{\partial \theta_s}{\partial z^*} + \frac{v^*}{Ar}\cdot\frac{\partial \theta_s}{\partial r^*}\right) = \frac{1}{Pe_s}\left[\frac{\partial^2 \theta_s}{\partial z^{*2}} + \frac{1}{Ar^2}\frac{\partial\left(r^*\frac{\partial \theta_s}{\partial r^*}\right)}{r^*\cdot\partial r^*}\right] + \left[(\theta_s - \theta_r)\cdot(r_g' - r_a) + \beta\right]\frac{\partial \Omega}{\partial \tau} \tag{22}$$

$$\Lambda_1\frac{\partial \omega}{\partial \tau} - \Lambda_2\frac{\partial \theta_s}{\partial \tau} = \frac{\partial}{\partial z^*}\left[\frac{1}{Pe_s'}\frac{\partial \omega}{\partial z^*} + \frac{1}{Ar^2}\cdot\frac{1}{r^*}\frac{\partial}{\partial r^*}\left(\frac{r^*}{Pe_s'}\frac{\partial \omega}{\partial r^*}\right)\right] - \frac{\partial \Omega}{\partial \tau} \tag{23}$$

where the following dimensionless variables are introduced:

$$\tau = \frac{V_{max}\cdot t}{L}, \quad z^* = \frac{z}{L}, \quad r^* = \frac{r}{R}, \quad \omega = \frac{P - P_0}{\Delta P},$$
$$\Omega = \frac{\bar{q}}{q_{max}}, \quad \theta_s = \frac{T_s - T_0}{\Delta T}, \quad \theta_m = \frac{T_m - T_0}{\Delta T},$$
$$\theta_f = \frac{T_f - T_0}{\Delta T}, \quad u_f^* = \frac{u_f}{V_{max}}, \quad u^* = \frac{u}{V_{max}}, \quad v^* = \frac{v}{V_{max}}$$

The dimensionless parameters are defined as follows:

$$Ar = \frac{R}{L}, \quad Pe_s = \frac{V_{max}L\rho_s C_{ps}}{\lambda_s}, \quad Pe_m = \frac{V_{max}L\rho_m C_{pm}}{\lambda_m},$$
$$Pe_f = \frac{V_{max}L\rho_f C_{pf}}{\lambda_f}, \quad Pe_s' = \frac{V_{max}L\rho_s q_{max}\mu}{\Delta P\cdot\rho_g K_{ap}},$$
$$r_g = \frac{\rho_g C_{pg}}{\rho_s C_{ps}}, \quad r_a = \frac{C_{pa}}{C_{ps}}\cdot q_{max}, \quad r_g' = \frac{C_{pg}}{C_{ps}},$$
$$\theta_R = \frac{T_0}{\Delta T}, \quad \omega_R = \frac{P_0}{\Delta P}, \quad \beta = \frac{\Delta H\cdot q_{max}}{\Delta T\cdot C_{ps}},$$
$$\Lambda_1 = \frac{\varepsilon\cdot\rho_g}{\rho_s(\omega + \omega_R)q_{max}}, \quad \Lambda_2 = \frac{\varepsilon\cdot\rho_g}{\rho_s(\theta_s + \theta_R)q_{max}}$$

3. Numerical method

The governing equations are solved by using the finite volume method described in detail by Patanker [12]. In the computational domain, a two-dimensional, non-uniform and staggered grid is used with a control volume formulation. The convection terms are discretized by using the power law scheme, the diffusion terms are discretized by the central difference scheme and the unsteady terms are discretized by the forward difference scheme. This algorithm provides a remarkably successful implicit method for simulating heat transfer in fluid flow. The discretized equations are solved by the line-by-line procedure, which is a combination of the Tri-Diagonal Matrix Algorithm (TDMA) and the Gauss–Seidel iteration technique.

Under-relaxation factors are employed to avoid divergence in the iterative solution of strongly nonlinear phenomena. The under-relaxation factors for pressure and temperature are set to 0.5 and 0.8, respectively.

The influence of time step and grid size on the model results were analyzed to assess whether the time step and grid size employed are acceptable. Based on the grid and time independent analysis, a time step between 0.02 and 0.2 and 24×40 grids were chosen to ensure the reliability of the results. The convergence criterion used in this method is 10^{-6}.

Table 1
Parameter values and operating conditions used in the model

Name	Symbol	Value
Average velocity of heat exchange fluid	$\bar{u}_f$	1 m s^{-1}
Adsorption temperature	T_a	318 K
Generation temperature	T_g	473 K
Fluid inlet temperature during heating	T_{hin}	493 K
Fluid inlet temperature during cooling	T_{cin}	298 K
Evaporator temperature	T_e	279 K
Condenser temperature	T_c	318 K
Density of adsorbent	ρ_s	620 kg m^{-3}
Specific heat of adsorbent	C_{ps}	836 J kg^{-1} K^{-1}
Thermal conductivity of adsorbent	λ_s	0.2 W m^{-1} K^{-1}
Heat of adsorption	ΔH	3.2×10^6 J kg^{-1}
Particle diameter	d	0.2 mm
Internal radius of metal tube	R_0	0.020 m
External radius of metal tube	R_1	0.021 m
External radius of adsorbent bed	R	0.036 m
Length of adsorbent bed	L	0.60 m
Macro-porosity of adsorbent bed	ε_a	0.38
Micro-porosity of adsorbent particle	ε_i	0.42

4. Results and discussion

A computer program was written based on the numerical methodology mentioned above to solve the model. Some base parameters used in the model are listed in Table 1. The effect of these parameters on the performance of the combined heat and mass recovery cycle will be discussed in the following sections. Since the mass recovery phase can be completed very quickly [9], the following discussions are based on 99% of the mass recovery process being fulfilled.

4.1. Degree of the heat recovery

From the authors' previous work [9], it was established that the temperature gap between the two adsorbers will decrease with an increase in heat recovery time. It was also mentioned there is less heat recovery produced with the increase of heat recovery time. When the temperature gap becomes zero, heat recovery will be completed since no heat energy can be produced. Here we define a parameter, D_{hr}, to describe the degree of the fulfillment of the heat recovery process:

$$D_{hr} = \left(1 - \frac{\Delta T}{T_g - T_a}\right) \times 100\% \tag{24}$$

where ΔT is the temperature gap between the two adsorbers, T_g is the generation temperature and T_a is the initial adsorption temperature.

Fig. 3 shows the variation of degree of heat recovery and heat recovery power with heat recovery time. It can be seen that D_{hr} increases quickly with heat recovery time at the beginning of heat recovery. However, when D_{hr} is greater than 90%, the rate of increase slows down. At that time, the value of the heat recovery power is less than 10% of the maximum value. From Fig. 4, it can be seen that when D_{hr} becomes greater than 90%, the marginal increase in COP brings about a severe decrease in SCP. This is due to the much smaller heat exchange rate between the two beds when the degree of the heat recovery process is over 90%. A small increase in COP will lead to a large increase in the heat recovery time, which in turn increases the total cycle time significantly.

4.2. Driven temperature

The driven temperature is defined as the temperature of the heat exchange fluid. In this analysis, a constant temperature difference of 20 K is maintained between the generation temperature and the driven temperature. The variations of COP and SCP with driven temperature at different degrees of heat recovery are shown in Figs. 5 and 6, respectively. It can be seen that both COP and SCP increase with an increase in the driven temperature of heat

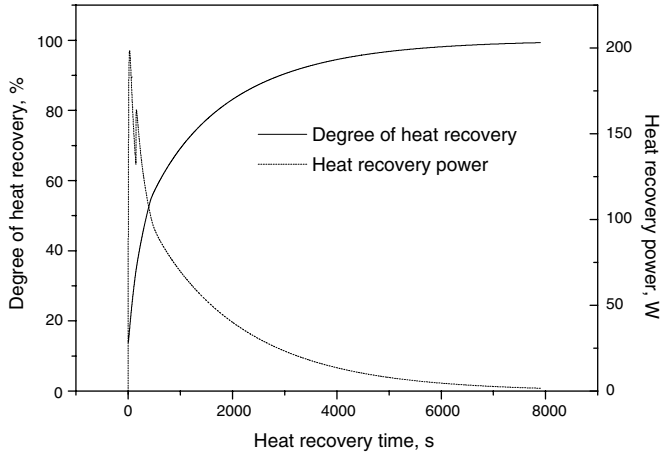

Fig. 3. Variation of degree of heat recovery and heat recovery power with heat recovery time.

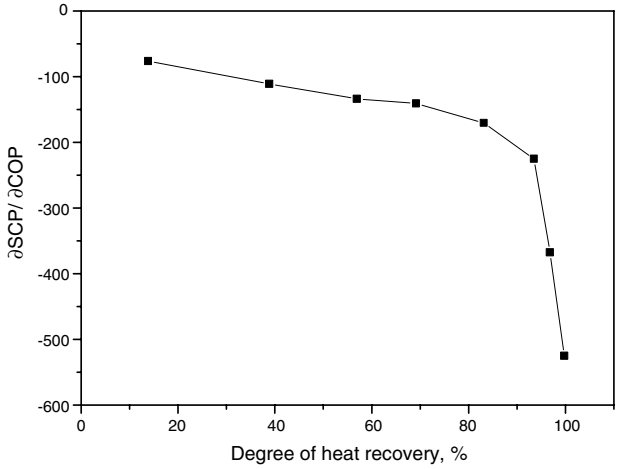

Fig. 4. Variation of ∂SCP/∂COP with degree of heat recovery.

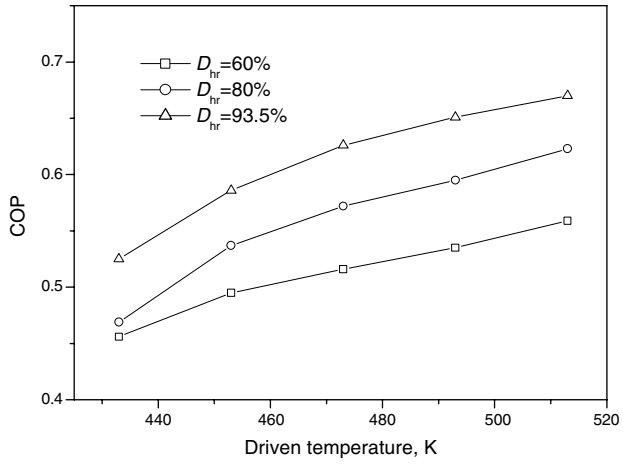

Fig. 5. Variation of COP with driven temperature.

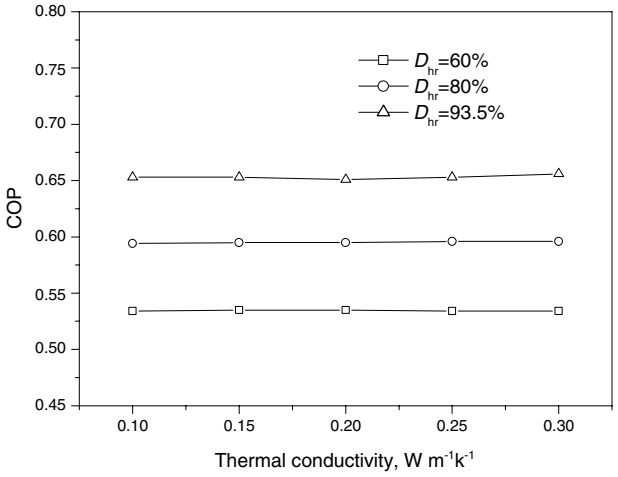

Fig. 7. Variation of COP with thermal conductivity of adsorbent bed.

exchange fluid which will in turn lead to an increase in the generation temperature. The COP of the basic cycle will increase with an increase in the generation temperature [13]. From the simulation results, the ratio of heat recovery energy to heat input of the basic cycle will increase with generation temperature for the same degree of heat recovery. The heat recovery process reduces the value of the heat input from external heat source but does not change the value of the cooling energy. Hence, the COP of the combined heat and mass recovery cycle becomes larger for a higher driven temperature. The cycle mass of refrigerant will increase with an increase in the generation temperature. Therefore, the cooling energy will also increase. Since the total cycle time does not increase very much with the increase of driven temperature of the heat exchange fluid, the value of SCP also increases. Although a high driven temperature can improve the system performance, safety issues and heat loss for the high temperature heat exchange fluid need be addressed in actual applications.

4.3. Thermal conductivity of adsorbent bed

Many researchers [14–16] have investigated the enhancement of heat transfer in the adsorbent bed in order to improve the performance of adsorption cooling systems. One way to enhance the heat transfer in the adsorbent bed is to use adsorbents of higher thermal conductivity. Figs. 7 and 8 show the variations of COP and SCP with thermal conductivity of the adsorbent bed for a combined heat and mass recovery cycle. It can be seen from Fig. 7 that thermal conductivity has negligible effect on the magnitude of the COP but it has a significant effect on the SCP. This is primarily because of the fact that the bed thermal conductivity has no effect on the heat input and cooling energy produced under fixed operating temperatures. In addition, the heat transfer rate between the adsorbent bed and heat exchange fluid will increase with an increase in the thermal conductivity of adsorbent bed resulting in a reduction of cycle time. Thus, the value of SCP increases

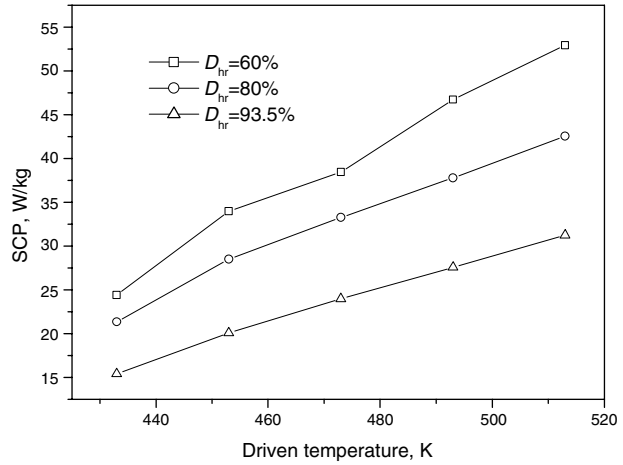

Fig. 6. Variation of SCP with driven temperature.

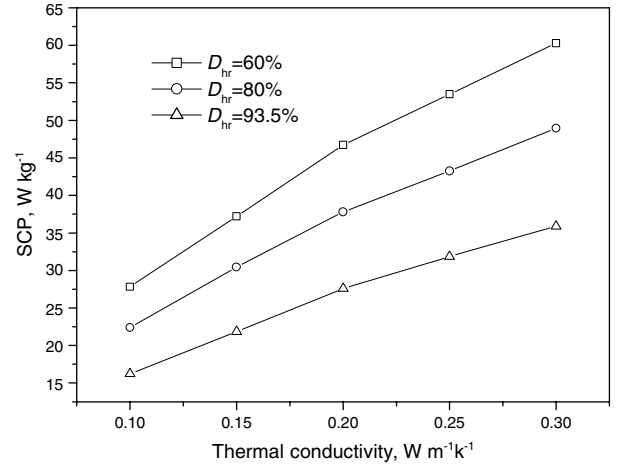

Fig. 8. Variation of SCP with thermal conductivity of adsorbent bed.

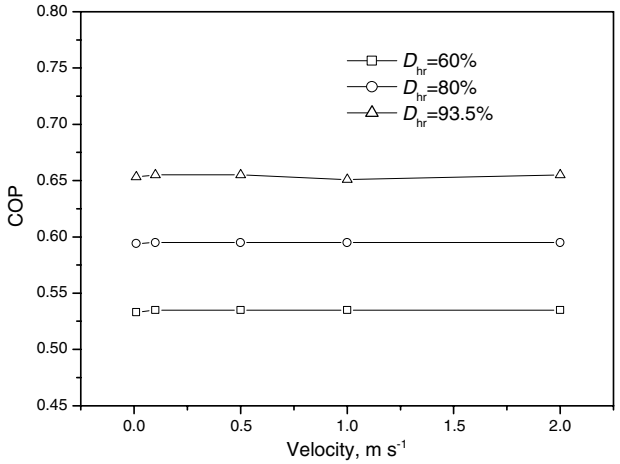

Fig. 9. Variation of COP with velocity of heat exchange fluid.

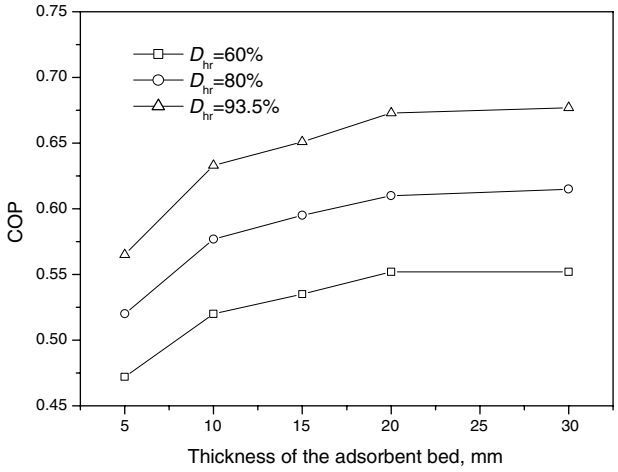

Fig. 11. Variation of COP with thickness of adsorbent bed.

with an increase in bed thermal conductivity. In general, an increase in thermal conductivity has a positive effect on the system performance of the combined heat and mass recovery cycle.

4.4. Velocity of heat exchange fluid

The effect of the velocity of heat exchange fluid on the performance coefficients are shown in Figs. 9 and 10. Since the heat input and cooling energy are not affected by the velocity of the heat exchange fluid, there will also be very little effect on the COP (see Fig. 9). When the fluid velocity is smaller than 0.01 m s^{-1}, the cycle time will increase very quickly with an increase in fluid velocity. The temperature gradient of the fluid inside the metal tube in the axial direction will increase for a lower fluid velocity. Therefore, the total heat exchange rate between the two beds and between the bed and external heat source will decrease, resulting in an increase in the cycle time. Hence, when the velocity is smaller than a certain value, the SCP deceases significantly with the reduction of velocity (Fig. 10). However, for velocities larger than 0.5 m s^{-1}, the cycle time does not change with velocity thus leading to negligible change in SCP. The optimal velocity of the heat exchange fluid should be in the range of 0.1–0.5 m s^{-1}.

4.5. Thickness of adsorbent bed

The adsorbent bed thickness is an important parameter that has great influence on the performance of an adsorption cooling cycle. Figs. 11 and 12 show the effect of bed thickness on the COP and SCP for a combined heat and mass recovery cycle. It can be seen that the COP increases with an increase in adsorbent thickness. On the contrary, the SCP reduces with an increase in adsorbent thickness. For a large thickness, the heat capacity ratio of the metal tube to adsorbent bed will decrease. This means that the heat input to the metal tube will decrease leading to an increase in COP. When the thickness is increased beyond a certain value, the heat energy consumed by the metal tube

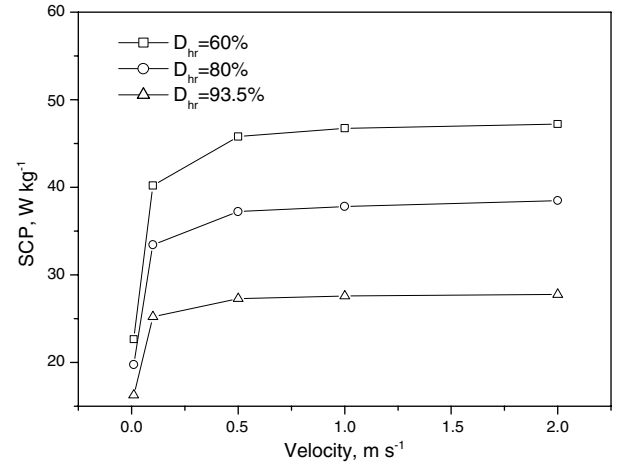

Fig. 10. Variation of SCP with velocity of heat exchange fluid.

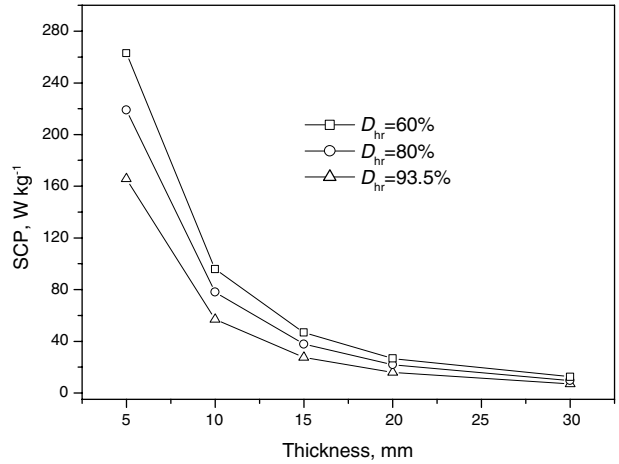

Fig. 12. Variation of SCP with thickness of adsorbent bed.

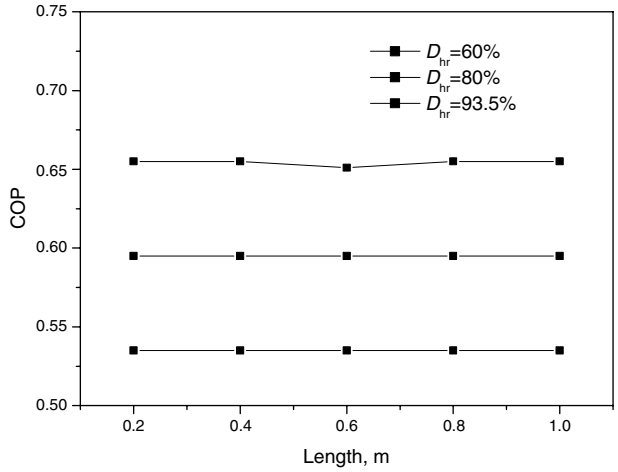

Fig. 13. Variation of COP with length of adsorbent bed.

is rather small compared with the total heat input. Therefore, the COP tends to a constant value for a large thickness of the adsorbent bed. Although a larger thickness means more adsorbate can be driven into cycling, the thermal resistance is also larger. Consequently, the heat exchange rate during the basic cycle process and heat recovery process is reduced contributing to a longer cycle time and a reduction in the SCP.

4.6. Length of adsorbent bed

Fig. 13 shows the effect of the length of adsorbent bed on the COP while Fig. 14 shows its effect on the SCP. It can be seen from Fig. 13 that the length of the adsorbent bed has no influence on the COP while the SCP shows a slight decline with an increase in the length of bed. For a certain degree of heat recovery, any change in the length of the adsorbent bed has negligible effect on heat input resulting in negligible change in the COP value. In this study, the velocity of heat exchange fluid is 1 m s^{-1}, which is higher than the optimal range mentioned in Section 4.4. The temperature gradient in the axial direction is very small. Hence, the increase in cycle time is negligible when the length of the bed increases. This leads to a slight change in the SCP. If the velocity of the fluid were to be reduced, an increase in the length of the adsorbent will result in a lower heat exchange rate per unit mass of adsorbent between two beds. The will in turn contribute to a longer cycle time and hence an obvious reduction in SCP.

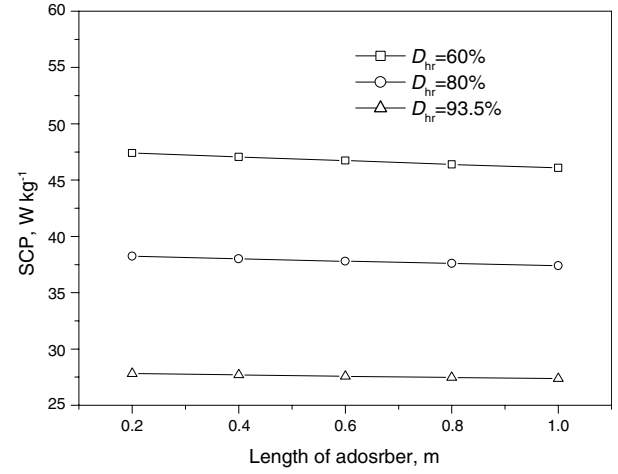

Fig. 14. Variation of SCP with length of adsorbent bed.

5. Conclusions

A parametric study of the system performance of a combined heat and mass recovery adsorption cooling system based on the zeolite 13X/water working pair was carried out by using a two-dimensional non-equilibrium numerical model. The following conclusions can be drawn:

1. The COP of the system increases while its SCP decreases with an increase in the degree of heat recovery (D_{hr}). When D_{hr} becomes greater than 90%, the increase of COP results in a severe decrease in the SCP.
2. Both COP and SCP increase with an increase in the driven temperature of heat exchange fluid. For very high driven temperatures, safety issues and heat loss should be addressed in actual applications.
3. Increasing the thermal conductivity of the bed can enhance the heat transfer in the adsorbent bed and reduce the cycle time. It has a positive effect on the system performance.
4. The SCP of the system can be severely deteriorated when the fluid velocity is below 0.1 m s^{-1}. However, for velocities larger than 0.5 m s^{-1}, any change in fluid velocity will result in negligible change in the SCP. The optimal velocity of the heat exchange fluid lies within the range of 0.1–0.5 m s^{-1}.
5. The COP of the system increases while its SCP decreases with an increase in adsorbent bed thickness. The SCP shows a slight decline with an increase in the length of adsorbent bed within the range of investigation.

References

[1] G. Cacciola, G. Restuccia, Reversible adsorption heat pump: a thermodynamic model, Int. J. Refrig. 18 (1995) 100–106.
[2] B.B. Saha, S. Koyama, T. Kashiwagi, A. Akisawa, K.C. Ng, H.T. Chua, Waste heat driven dual-mode, multi-stage, multi-bed regenerative adsorption system, Int. J. Refrig. 26 (2003) 749–757.
[3] R.E. Critoph, Forced convection adsorption cycles, Appl. Therm. Eng. 18 (1998) 799–807.
[4] D.J. Miles, Analysis and design of a solid adsorption heat driven heat pump, Ph.D. thesis, Georgia Institute of Technology, 1989.
[5] W. Wang, T.F. Qu, R.Z. Wang, Influence of degree of mass recovery and heat regeneration on adsorption refrigeration cycles, Energy Convers. Manage. 43 (2002) 733–741.
[6] R.Z. Wang, Performance improvement of adsorption cooling by heat and mass recovery operation, Int. J. Refrig. 24 (2001) 602–611.
[7] T.F. Qu, R.Z. Wang, W. Wang, Study on heat and mass recovery in adsorption refrigeration cycles, Appl. Therm. Eng. 21 (2001) 439–452.

[8] F. Poyelle, J.J. Guilleminot, F. Meunier, Experimental tests and predictive model of an adsorptive air conditioning unit, Ind. Eng. Chem. Res. 38 (1999) 298–309.
[9] K.C. Leong, Y. Liu, Numerical study of a combined heat and mass recovery adsorption cooling cycle, Int. J. Heat Mass Transfer 47 (2004) 4761–4770.
[10] D. Zhu, S. Wang, Experimental investigation of contact resistance in adsorber of solar adsorption refrigeration, Sol. Energy 73 (2002) 177–185.
[11] N. Ben Amar, L.M. Sun, F. Meunier, Numerical analysis of adsorptive temperature wave refrigerative heat pump, Appl. Therm. Eng. 16 (1996) 405–418.
[12] S.V. Patankar, Numerical Heat Transfer and Fluid Flow, Hemisphere Publishing Corporation, New York, 1980.
[13] Y. Liu, K.C. Leong, The effect of operating conditions on the performance of zeolite/water adsorption cooling systems, Appl. Therm. Eng. 25 (2005) 1403–1418.
[14] M. Groll, Reaction beds for dry sorption machines, Heat Recov. Syst. CHP 13 (1993) 341–346.
[15] M. Pons, D. Laurent, F. Meunier, Experimental temperature fronts for adsorptive heat pump applications, Appl. Therm. Eng. 16 (1996) 395–404.
[16] L. Marletta, G. Maggio, A. Freni, M. Ingrasciotta, G. Restuccia, A non-uniform temperature non-uniform pressure dynamic model of heat and mass transfer in compact adsorbent beds, Int. J. Heat Mass Transfer 45 (2002) 3321–3330.